ACS OMEGA

Open Access

http://pubs.acs.org/journal/acsodf

Article

Qualitative and Quantitative Investigation of Biochar-Cu^0 Composite for Nickel Adsorption

Salah Ud Din,* Junaid Murtaza Awan, Muhammad Imran, Pervaiz Ahmad, Sirajul Haq, Sana Shakil, Kholoud Al-mugren,* Satam Alotibi, Abdulrahman I. Alharthi, Muhammad Sarfraz Khan, and Mayeen Uddin Khandaker

Cite This: *ACS Omega* 2023, 8, 39186−39193

Read Online

ACCESS | Metrics & More | Article Recommendations | Supporting Information

ABSTRACT: The current investigation deals with the treatment of water pollution that is caused by the leaching of nickel ions from the metallurgical industry and new-energy batteries. Therefore, an eco-friendly treatment of nickel through the use of a composite of cotton stalk biochar with nanozerovalent copper has been presented in this investigation signifying the impact of zerovalent copper in enhancing the adsorption capacity of biochar for nickel adsorption. Thermogravimetric analysis data showed the adsorbent to be significantly stable in the higher thermal range, whereas transmission electron microscopy analysis confirmed the particles to be 27 nm and also showed the cubic geometry of the particles. A much closer scanning electron microscopy analysis shows the morphology of particles to be cubic in shape. Batch adsorption indicated a positive influence of pH increase on adsorption due to the electrostatic attraction between positive nickel ions and post point of zero charge (pH_{PZC}) negative surface of copper biochar composite (pH > 5.5). A high adsorption rate was observed in the first 60 min, whereas adsorption increased with the increase in temperature from 303 to 318 K. Kinetic modeling confirmed the pseudo-first-order to fit best to the data. The apparent activation energy (11.96 kJ mol^{-1}) is indicative of the chemical nature of the process. The adsorption data fitted well to the Langmuir adsorption model. The negative values of apparent ΔG° and the positive values of apparent ΔH° indicate the spontaneity and endothermicity of the process, respectively, whereas the positive values of apparent ΔS° point toward increased randomness during the process. Postadsorption XPS suggests the adsorption of nickel on the surface of biochar composites in the form of $Ni(OH)_2$ and NiO(OH).

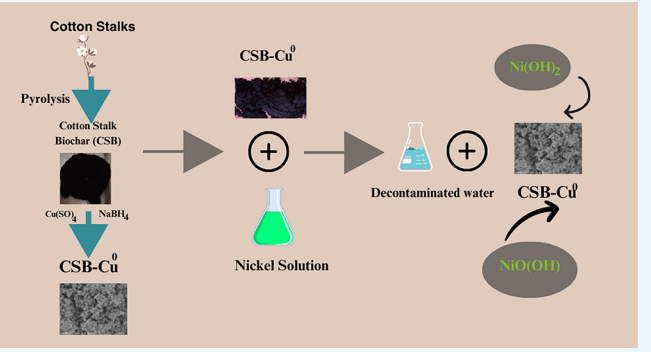

1. INTRODUCTION

Nickel being a poisonous heavy metal is of great concern for humans, animals, and plant species. Organic pollutants or dyes are mostly degradable, but ions of nickel are nondegradable in water. It remains in water in its toxic forms, and it is therefore necessary to remove nickel from water in order to make it fit for drinking purposes. Most of the compounds of nickel are in the +2 oxidation state. However, zero, + 3, and +4 oxidation state compounds are also found in nature as $Ni(CO)_4$,[1] $[Ni(phen)_3]^{+3}$, and Cs_2NiF_6.[2] It forms many large complexes, most of which are colored green or blue. Laterites, including limonite, pentlandite, and garnierite, are its prevalent mineral.[2]

Nickel is a pollutant commonly generated from metal mining, electroplating, industries producing fat, agricultural processes, as well as urban and other activities. Major sources of nickel are the largest base metal smelter.[3] Ni may be released into groundwater from rocks that contain nickel, but the main source of nickel is from plumbing materials that leach nickel in sources of drinking water.[2,4] One of the most frequent ways that people get exposed is via eating or drinking contaminated food or water, as well as breathing in polluted ambient air.[5,6] The maximum permitted limit of Ni^{2+} in drinking water is 0.5 mg L^{-1}. Ni^{2+} can cause headache, dermatitis, nausea, and dizziness and can even cause cancer in human beings. Daily uptake of nickel in food by humans is about 0.1−0.3 mg.[7] The respiratory system, particularly the nasal cavities, sinuses, and skin, and vital organs are mostly damaged by exposure to nickel. It is found that nickel-plating workers, who are more exposed to nickel, mostly suffer from asthma. Many other respiratory effects caused by nickel exposure include chronic rhinitis, bronchitis, diaphragm nose erosion, decreased lung capacity, and increased respiratory rate. Skin is highly susceptible to nickel and its compounds,

Received: June 22, 2023
Accepted: September 28, 2023
Published: October 11, 2023

causing inflammation, eczema, and allergic dermatitis.[8] Nickel poisoning can cause headache, breakdown, nausea, vomiting, and extreme pneumonia.[9] Rhinitis, nasal perforation, and bronchial asthma are the symptoms that are mostly observed in nickel refiners and workers.

Various techniques are in use for the decontamination of heavy metals from water such as filtration, coagulation, membrane separation, precipitation, and so forth. However, due to its efficiency, cost-effective nature, and simplicity, adsorption has become the most suitable and preferred way to eradicate heavy metal ions from aqueous solution as compared to other techniques. Due to the porosity in structure and the unique surface chemistry, various carbon materials like carbon nanotubes[10] and graphene[11] have been found to show a strong affinity for heavy metals from aqueous solution. However, due to their high cost, their application in water treatment is limited. Biochar, because of its high porosity and heterogeneous surface chemistry, has a good adsorption affinity for heavy metals. The extra availability of biochar makes it cheaper as compared to activated carbon,[12,13] thus justifying it as a superior adsorbent among water treatment options in the developing countries.

Biochar's ability to adsorb pollutants depends on its physiochemical parameters, which vary greatly from raw materials to pyrolysis conditions.[14] Nevertheless, excessive heating of biochar leads to a decrease in the adsorption sites, thereby decreasing the sorption capacities. This problem of a decrease in adsorption capacities has been addressed by compositing biochar with iron manganese[15,16] and magnesium.[17,18] However, the composites of zerovalent copper are reported to be mechanically more stable in comparison to the aforementioned composites of biochar.[19] Moreover, zerovalent copper can potentially increase the surface sites and surface functionalities of raw biochar, making it more favorable for the adsorption of nickel ions. Additionally, impregnation of copper may also change the oxidation state of nickel ions during the adsorption process, making it suitable for adsorption on the biochar surface and thereby increasing the adsorption capacity of the adsorbent.

Farmers in the field routinely burn large quantities of cotton stalks. Subsequently, significant amounts of greenhouse gases are released into the atmosphere (e.g., carbon dioxide, carbon monoxide, ammonia, nitrogen oxides, and sulfur dioxide).[20] Recycling crops, such as cotton stalk in this investigation, is, therefore, an important need for value-added goods in order to protect the environment from different hazards. This study, therefore, combines zerovalent copper (Cu^0) with cotton stalk biochar (CSB) in the form of a more ecofriendly and stable composite to eliminate nickel with high efficiency and cost-effectiveness.

2. MATERIALS AND METHODS

2.1. Synthesis of Composite of CSB with Cu^0 (CSB-nZVCu). Scanning electron microscopy (SEM) of CSB with Cu^0 was performed using a NOVA FEISEM_450 microscope. The composite of CSB with Cu^0 was prepared by the method reported earlier.[19] Washed biomass of cotton stalk was pyrolyzed to 400 °C at 8 °C/min to prepare biochar. Pulverized CSB (0.25 g) was mixed with a 50 mL solution of copper sulfate (0.1 M) for 10 min and afterward titrated with 50 mL solution of sodium borohydride (0.2 M) dropwise to synthesize the composite of CSB-zerovalent copper (CSB-nZVCu). After centrifugation and oven drying, the composite was heated for 30 min at 300 °C before applying it for the adsorption of nickel.

2.2. Characterization of Biochar Composite. The shape and size of the composite of CSB with Cu^0 were studied using TEM (JEOL JEM 2100). Thermogravimetric analysis (TGA) of CSB-nZVCu was performed under an air stream at a heating speed of 10 °C/min using the TGA/DSC1 thermogravimetric analyzer from Mettler Toledo.

The pH_{pzc} (point of zero charge) of the sample was measured by using the pH drift method.[21] Forty milliliters of 0.1 M NaC1 solution was taken in various flasks, and the initial pH (2−11) was adjusted in these flasks by adding 0.1 M NaOH/HCl solutions as pH adjusting reagents. Later on, to each flask was added 0.1 g of CSB composite, and the flasks were shaken for 24 h in a shaker bath (GFL 1086) at 298 K. The final pH was recorded after 24 h of shaking, and the difference between the initial pH and final pH (ΔpH) was calculated. In order to determine the PZC value, a graph was plotted between ΔpH and initial pH, and the line crossing the zero (of ΔpH) was taken as the PZC.

2.3. Adsorption Studies and Kinetic Modeling. Batch mode experiments were conducted to explore the potential of the CSB-nZVCu composite for nickel adsorption as a function of concentration, solution pH, and temperature. The effect of solution pH vs Ni removal was investigated by adding CSB-nZVCu (0.1 g) into different flasks containing 70 mg L^{-1} of Ni solution (40 mL) maintained at a temperature of 303 K. The solution's pH was then modified with HNO_3/NaOH (0.1 M) solutions between 2 and 8. For studying the temperature effect in the range of 303 to 318 K, similar conditions of concentration and adsorbent dose, that is, 10−90 mg L^{-1} and 0.1 g, respectively, were applied at pH 5. These flasks containing the suspensions were afterward shaken in a shaker bath at 120 rpm. After 12 h, the solid biochar composite was separated from the solutions through a Whatman filter paper (no. 43), and the liquid filtrates were then checked for the remaining Ni through an atomic absorption spectrophotometer.

Kinetics of nickel adsorption on the biochar composite was studied in the temperature range of 303−318 K and at pH 7. Several flasks having Ni solutions (40 mL of 70 mg L^{-1}) and 0.1 g of the adsorbent were shaken in a shaker bath for different intervals up to 24 h. These flasks at different times were then checked for final pH before filtration and afterward were analyzed for remaining Ni through an atomic absorption spectrophotometer.

The pseudo-first-order kinetics eq 1 and pseudo-second-order eq 2 were applied to the kinetic data of nickel adsorption on the biochar composite:

$$\log(q_e - q_t) = \log(q_e) - \frac{k_1 t}{2.303} \quad (1)$$

$$\frac{t}{q_t} = \frac{1}{(k_2 q_e^2)} + \frac{t}{q} \quad (2)$$

where q_e and q_t denotes the adsorbed nickel at equilibrium and at any time, respectively, whereas k and k_2 are the pseudo-first- and pseudo-second-order rate constants.

3. RESULTS AND DISCUSSION

3.1. Characterization. The composite of Cu^0 with CSB was characterized using various techniques. TEM micrographs

https://doi.org/10.1021/acsomega.3c04456
ACS Omega 2023, 8, 39186−39193

are shown in Figures 1A,B and S1 to analyze the particle size and shape of the copper biochar composite. The image shows

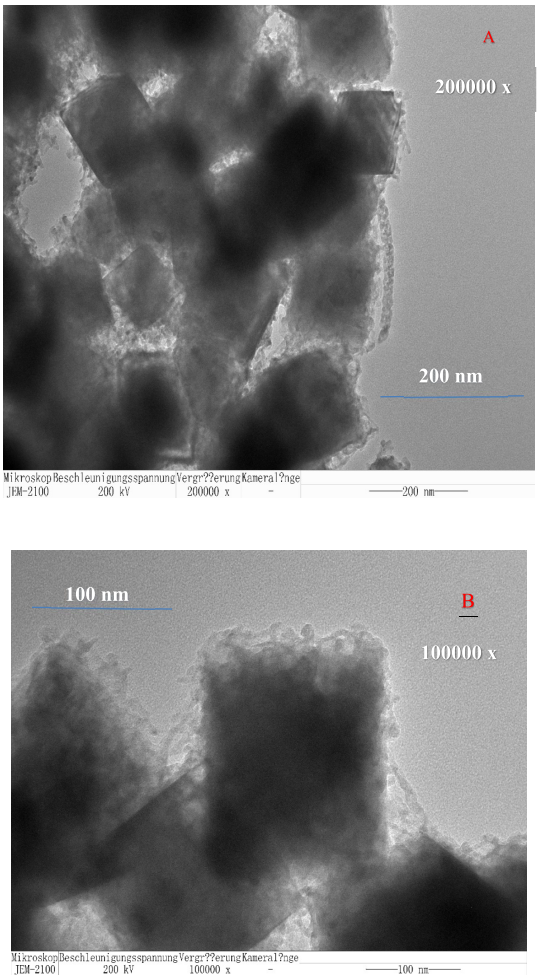

Figure 1. TEM images of CSB-nZVCu at magnifications of 200000× (A) and 100000× (B).

the cubic form of the particles. The dark spots on the particle indicate the presence of copper.[22] The average particle size calculated by using the equation in ImageJ software as shown in Figure S1 was about 20.5 nm (xc is the average particle size inside Figure S2), which is almost equal to the particle size calculated from XRD by using the Scherrer equation.

SEM micrographs of the nanocomposite of Cu^0 with CSB were obtained at much closer magnifications as shown in Figure 2. From the micrographs' scale, it is clear that the particles are in the nanometer range and uniform in size and having a cubic morphology. Moreover, the small particles can be seen sticking to the surface of biochar, which indicates that zerovalent copper is evenly dispersed on the surface of biochar.

CSB-nZVCu was also subjected to TGA to understand their thermal resistance and pyrolytic activity. Figure 3 shows the thermal stability of CSB-nZVCu with the help of TGA curves and weight loss differential (DSC) calculations. The 3% weight loss up to 130 °C was attributed to the release of water from CSB-nZVCu.[23] The breakdown of lignin and carbohydrates takes place in the range of 300−700 °C which is supported by the appearance of a broad endothermic DSC curve in this range[24] as indicated by the 25% weight loss in this region. The slower weight loss after 700 °C that is also accompanied by an

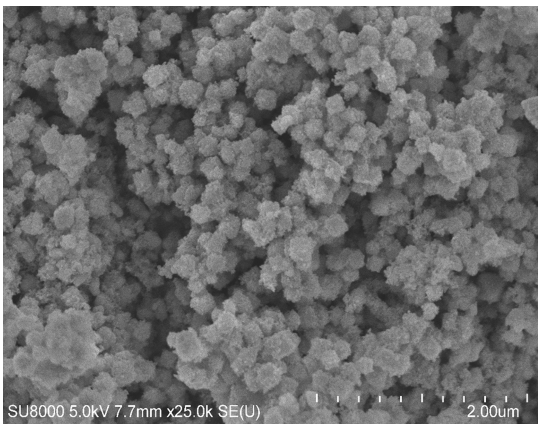

Figure 2. SEM images of CSB-nZVCu at 7.7 mm x 25.0k.

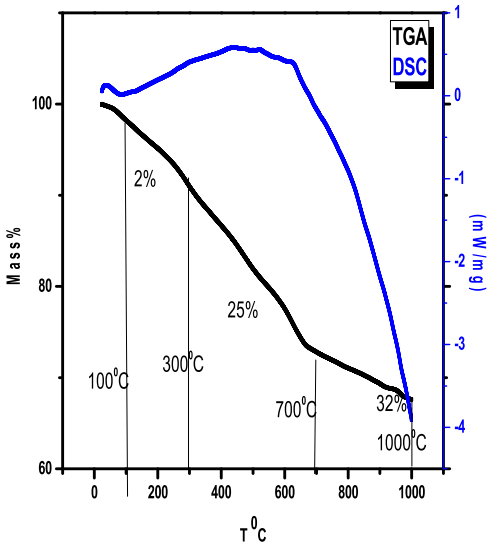

Figure 3. TGA of CSB-nZVCu.

exothermic DSC curve beyond this temperature can be due to the oxidation of zerovalent copper to copper oxide (volatile) or breakdown of organic matter, which results in weight loss as well as in the release of heat. The stability of the composite up to 130 °C with only 3% weight loss indicates the composite's stability for retaining water, which in turn is beneficial for sustaining its adsorption capacity for nickel removal from aqueous solutions. The breakdown of organic compounds in the higher-temperature regions indicates the presence of different organic functional groups on the composite's surface, which may take part in the adsorption of nickel. It is confirmed from the TGA/DSC curves that the biochar with the Cu composite is robust and heat resistant even at a high temperature of 1000 °C with a total weight loss of only 35%. The biochar consisted of a more stable form of carbon with greater resistance as the pyrolysis temperature rose.

The sample's pHpzc (PZC) was measured using the method of pH drift.[21,25] In order to determine the PZC values, a graph was plotted between ΔpH and initial pH, and the line crossing the zero (of ΔpH) was taken as PZC, and it comes out to be 5.5 as shown in Figure 4. The PZC value indicates that the surface of the composite is positive below pH 5.5 due to protonation of the surface functional groups, and this pH range is suitable for attractive interactions with the negative metal ions. The increase in pH above 5.5 creates more negative

https://doi.org/10.1021/acsomega.3c04456
ACS Omega 2023, 8, 39186−39193

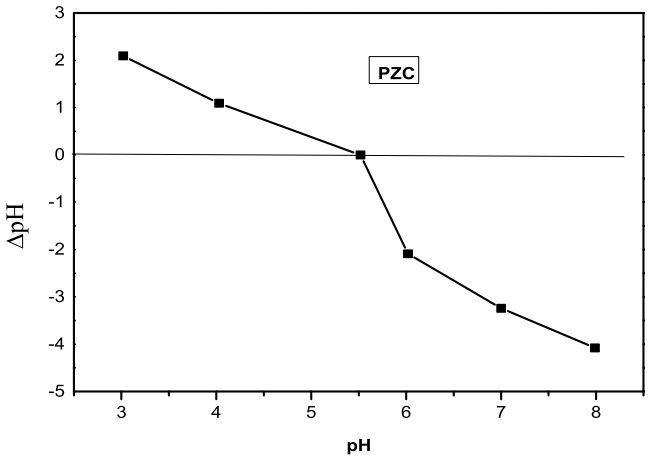

Figure 4. PZC of CSB-nZVCu.

surface charge on the surface due to deprotonation of the surface functional groups which may electrostatically attract the positively charged cations such as nickel. The PZC value therefore proves the suitability of this composite for the pH range of drinking waters (6.5−8.5) for nickel adsorption.

In our previous work,[26] we have reported the XRD, SEM, XPS, and FTIR of this composite of Cu^0 with CSB. XRD confirmed the presence of Cu^0 peaks, which was also supported by the XPS studies, and such peaks are absent in the amorphous virgin CSB (Figure S3), whereas the crystallite size calculated using the Scherrer equation was 27.97 nm. SEM supported the cubic morphology and porous structure of the sample as compared to the less porous structure of the virgin CSB (Figure S4), while the FTIR peak in the range of 600−625 cm^{-1} was due to the presence of Cu−O vibration.

3.2. Adsorption Studies. In a controlled screening test, nickel was adsorbed (initial nickel concentration 30 mg L^{-1} at pH 5 and at 318 K) on the surface of CSB and a composite of Cu^0 with CSB, as shown in Figure S5. As is clear from the figure, there was a higher adsorption of nickel ions (97%) observed on the composite of Cu^0 with CSB as compared to the virgin CSB which shows the enhanced adsorptive effect of modification on CSB for nickel removal. This enhanced adsorptive effect of the composite is due to the synergic effects of both Cu^0 and CSB for nickel adsorption as well as the increase in the porosity of the composite as compared to the virgin biochar, as is clear from the SEM images. Further study for nickel adsorption therefore proceeded only on the composite of Cu^0 with CSB.

3.3. Effect of Contact Time on Nickel Adsorption. The effect of the contact time on the adsorption of nickel ions was studied at pH 7 with a nickel concentration of 70 mg L^{-1} and at 303 K. As shown in Figure 5, the graph is plotted against time (min) vs X (mol g^{-1}). The graph shows the high adsorption rate in the early 60 min due to the large number of active sites being accessed, and the rate then decelerates steadily in the later hours due to competition of nickel ions for the limited number of adsorption sites. Four hours were taken as the equilibrium time of the process according to the analysis of the figure.

3.4. Kinetic Modeling for Nickel Adsorption. The kinetic data were subjected to pseudo-first- and pseudo-second-order models. The graphs shown in Figures 6 and S6 show that the data best followed the pseudo-first-order equation in the case of nickel adsorption on copper biochar

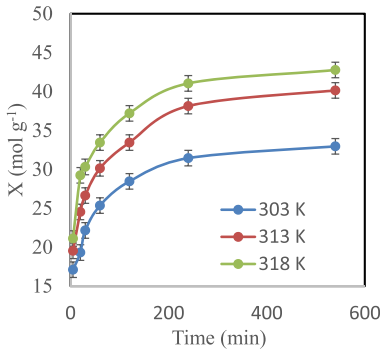

Figure 5. Effect of contact time on nickel adsorption on CSB-nZVCu.

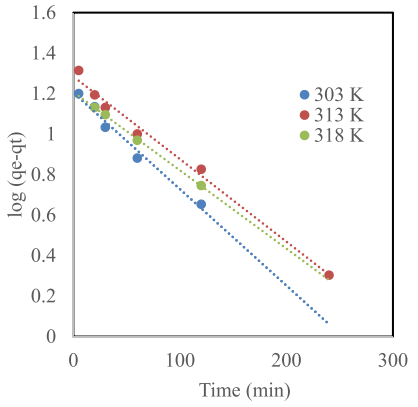

Figure 6. Pseudo-first-order kinetics for nickel adsorption on CSB-nZVCu.

composite. The applicability of the pseudo-first-order equation to the data shows the process of nickel adsorption on zerovalent biochar composite to be diffusion-limited in nature, and the pseudo-first-order rate constants are given in Table 1.

Table 1. Pseudo-First-Order Parameters and Apparent Activation Energy (*Ea*)

temperature (K)	$k \times 10^3$	R^2	*Ea* (kJ mol^{-1})
303	11.05	0.98	11.59
313	9.212	0.99	
318	8.982	0.99	

3.5. pH Effect on Nickel Adsorption. The pH effect on nickel adsorption is also studied at pH = 2−8 (to avoid precipitation at higher pH) and at an initial nickel concentration of 70 mg L^{-1}, as shown in Figure 7. The figure shows an increasing trend of adsorption with the increase in pH with the maximum adsorption of 45.42 × 10^5 mol g^{-1} which can be explained with the help of the PZC of the copper biochar composite. The figure shows that the increase of pH increases the adsorption due to electrostatic attraction between positive nickel ions and post-PZC (pH > 5.5) negative surface of copper biochar composite, as shown in Figure 4. Reduced adsorption in the lower pH range is conversely due to electrostatic repulsion between nickel ions and the positive surface below the PZC. Moreover, competition between H^+ ions and Ni^{2+} ions for the surface may also lead to reduced adsorption in the acidic pH range. A similar trend of adsorption of nickel is reported in the literature.[14]

https://doi.org/10.1021/acsomega.3c04456
ACS Omega 2023, 8, 39186−39193

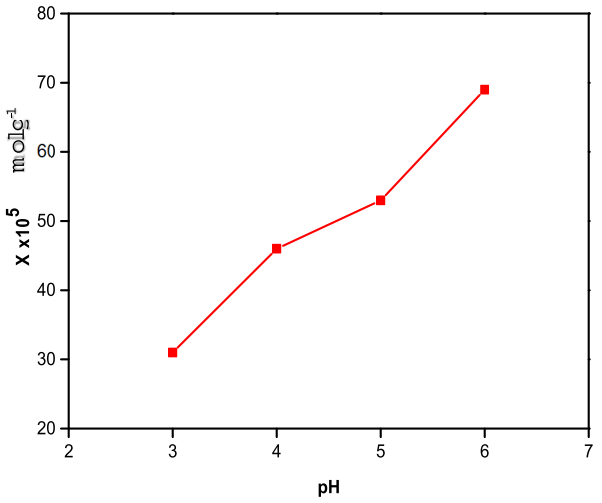

Figure 7. Effect of pH on nickel adsorption on CSB-nZVCu.

3.6. Concentration and Temperature Effect on Nickel Adsorption. Temperature and concentration effect on nickel adsorption by the biochar composite surface is investigated by varying the temperature in the range of 303−318 K and in the concentration range of 10−90 mg L^{-1} as shown in Figure 8.

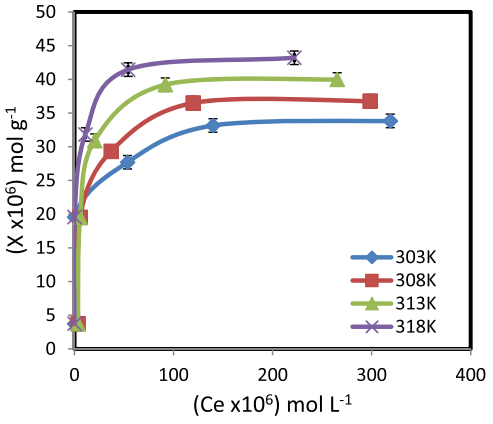

Figure 8. Effect of temperature on nickel adsorption on CSB-nZVCu.

There was an initial increasing trend of adsorption in the initial concentration range, which slowed as the concentration further increased, finally coming to an equilibrium, and the curve turned flat. Increased concentration of nickel ions versus the limited number of adsorption sites can be the reason for lower adsorption, leading to an equilibrium condition. Also, the adsorption of nickel on the biochar surface increased from 34.12 to 43.48 mol g^{-1} with the increase in temperature to 318 K. This increase of adsorption is attributed to more surface sites that were created due to breakage of bonds on the surface of the adsorbent in addition to an increased diffusion rate of nickel ions onto the adsorbent surface.

3.7. Langmuir Model for Nickel. For nickel adsorption on copper composite biochar surface, the Langmuir model is applied in the temperature range of 303−318 K as shown in Figure 9 according to the following equation.

$$\frac{Ce}{X} = \frac{1}{X_{max} \times K_b} + \frac{Ce}{X_{max}} \quad (3)$$

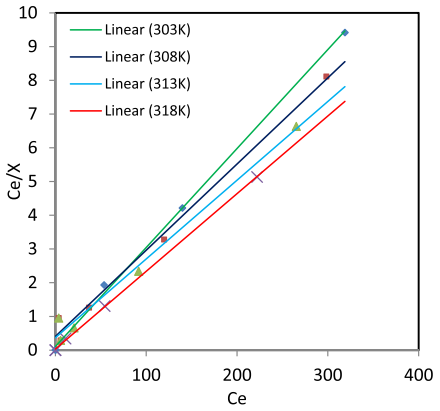

Figure 9. Langmuir model for nickel adsorption on CSB-nZVCu.

Here, *Ce*, *X*, and K_b indicate the equilibrium concentration of the adsorbate, adsorbed nickel, and binding energy constant, respectively.

The high values of R^2 (>0.98) indicate that for nickel adsorption on the biochar copper composite surface, the data fitted well to the Langmuir model. Within the temperature range studied, the increase of adsorption capacity (X_m) from 34 × 10^6 to 43 × 10^6 mol g^{-1} and the binding energy constant (K_b) obtained from the model (Table 2) show the endothermic nature of the process and also suggest increasing number of surface sites to increase the temperature as discussed in Section 3.6. The range of adsorption capacity reported in the current investigation as shown in Table 3 is higher than the adsorption capacities reported in the literature.[27,28]

Table 2. Langmuir Parameters for Nickel Adsorption on CSB-nZVCu at pH 5

temp (K)	$X_m \times 10^5$ (mol g^{-1})	$K_b \times 10^{-5}$ (L mol^{-1})	R^2
303	34.12	0.264	0.99
308	39.21	0.063	0.99
313	42.92	0.063	0.98
318	43.48	0.640	0.99

3.8. Apparent Activation Energy. The apparent activation energy (*Ea*) of nickel adsorption on the Cu^0-biochar composite was calculated by applying the Arrhenius equation to the kinetic data in the form

Table 3. Comparison of the Adsorption Capacities of Different Adsorbents for Ni

adsorbent	X_m (mg g^{-1})	references
kaolinite-supported zerovalent iron nanoparticles	9.24	29
chemically modified brown algae	11.63	30
sawdust of *Dalbergia sissoo*	10.47	31
agro-waste walnut shell biochar	13.25	32
magnetic biochar derived from *Eichhornia crassipes*	0.489	33
compost	9	34
Chrysanthemum indicum derived biochar	29.44	35
wood vinegar treated secondary compost	28.7	36
rice straw biochar	13.34	37
present study for nickel on CSB-nZVCu	32.58	present study

https://doi.org/10.1021/acsomega.3c04456
ACS Omega 2023, 8, 39186−39193

$$\ln k = \ln A - \frac{Ea}{RT} \quad (4)$$

where T (K), R, k, A, and Ea represent the temperature, the general gas constant, the rate constant, the pre-exponential factor, and the apparent activation energy, respectively. The apparent activation energy (11.96 kJ mol^{-1}) was obtained from the slope of a plot of ln$k$ as a function of T^{-1} (Figure S7) which suggests the presence of a barrier to be crossed, and also its value is indicative of the chemical nature of the process (8.3−83.7 kJ mol^{-1}).[38]

3.9. Apparent Thermodynamic Parameters. Nickel adsorption data at varying temperatures were used to calculate the apparent thermodynamic parameters according to eqs 5 and 6 and are listed in Table 4

$$\ln K_b = \frac{\Delta S^\circ}{R} - \frac{\Delta H^\circ}{RT} \quad (5)$$

$$\Delta G^\circ = \Delta H^\circ - T\Delta S^\circ \quad (6)$$

Table 4. Apparent Thermodynamic Parameters for Nickel on CSB-nZVCu at pH 5

ΔH° (kJ mol^{-1})	ΔS° (J mol^{1})	ΔG° (kJ mol^{-1})			
		303 K	308 K	303 K	318 K
126.55	0.430	−3.8779	−6.0302	−8.1826	−10.335

Both ΔH° and ΔS° for nickel adsorption on Cu^0-biochar are obtained as the slope and intercept of a linear plot of eq 4 (Figure S8) where K_b (binding energy constant from Langmuir equation) and R (universal gas constant) are expressed in units of L mol^{-1} and J mol^{-1} K^{-1}, respectively. The obtained ΔH° and ΔS° were then used in eq 5 to calculate ΔG° (Table 4). The values of ΔH° and ΔS° obtained in the current study are positive which points toward the endothermic nature of adsorption and indicates the adsorption process to be accompanied by increased randomness, respectively. The negative values of ΔG° at all three temperatures indicate the feasibility and spontaneity of the process. Moreover, the increased negativity in ΔG° with the increase in temperature shows that the process becomes more and more favorable at higher temperatures. The trend of apparent thermodynamic parameters obtained in the present investigation matches well with the trend of thermodynamic parameters reported elsewhere.[28,39]

3.10. Mechanism of Nickel Adsorption on Biochar Composite. XPS study of nickel adsorption was performed to understand the adsorption mechanism of nickel on the surface of Cu^0-CSB. The resulting spectra are shown in Figure 10 that indicate the peaks of nickel confirming the adsorption of nickel on the surface of the biochar adsorbent. Further deconvolution of nickel spectra shows subpeaks at binding energies of 855.13 (Ni 2p$_3$), 857.10 (Ni 2p$_3$), 861.78 (Ni 2p$_3$), and 879.14 (Ni 2p$_3$) eV. These binding energy values of 855.13 and 857.10 suggest the adsorption of nickel on the surface of biochar composites in the form of Ni(OH)$_2$ and NiO(OH), respectively, whereas the rest of the peaks are satellite peaks.[40] The mechanisms of nickel adsorption on various adsorbents are reported either as inner sphere complexation, outer sphere complexation, ion exchange, or surface coprecipitation.[41−46] Nature of the adsorbent, pH range, and PZC are among the factors responsible for guiding the mechanism of nickel adsorption. In adsorbents with more hydroxyl-containing surface functional groups such as −COOH, surface coprecipitation, as observed in the present investigation, is mostly favored in which Ni is adsorbed as hydroxide and oxyhydroxides.[47] However, in adsorbents having ion-exchange properties, ion-exchange mechanism for nickel adsorption is observed. In the lower pH range, the adsorbent mostly adsorbs as outer-sphere complexation,[47] whereas at higher pH, inner-sphere complexation[48] and coprecipitation of nickel ions are mostly observed. Surface charge also plays an important role as the surface due to deprotonation has, in many cases, more hydroxyl surface sites than the protonated surface sites, resulting in a coprecipitation mechanism for nickel adsorption to occur.[49]

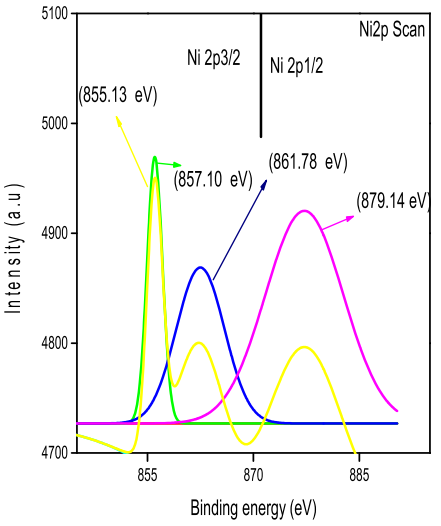

Figure 10. XPS Ni 2p spectra after adsorption on CSB-nZVCu.

4. CONCLUSIONS

Cu^0-composite with CSB was used for the adsorption of nickel from water. The adsorbent size calculated from TEM using ImageJ software was 21 nm. TGA confirmed high copper biochar composite stability at higher temperatures. PZC (5.5) shows the suitability of the adsorbent for nickel adsorption and also explains the higher adsorption of nickel on the adsorbent with the increase in pH. An equilibrium time of 240 min was settled for nickel, and the kinetic data obeyed the pseudo-first-order equation. Increasing the pH and temperature supports the adsorption of nickel on copper biochar. Nickle adsorption on copper biochar indicated monolayer adsorbate coverage by following the Langmuir model at all temperatures. The adsorbent's adsorption potential was found to be significantly higher for nickel, signifying the appropriateness of zerovalent copper composite with CSB to eliminate nickel from water.

■ ASSOCIATED CONTENT

Supporting Information

The Supporting Information is available free of charge at https://pubs.acs.org/doi/10.1021/acsomega.3c04456.

Characterization of the materials, comparative adsorption graph on CSB and CSB-Cu°, pseudo-second-order plot, Arrhenius plot, and Vant Hoff 's plot (DOCX)

https://doi.org/10.1021/acsomega.3c04456
ACS Omega 2023, 8, 39186−39193

AUTHOR INFORMATION

Corresponding Authors

Salah Ud Din − *Department of Chemistry, University of Azad Jammu and Kashmir, Muzaffarabad 13100 Azad Kashmir, Pakistan*; orcid.org/0000-0002-4450-7431; Email: salah.mahsud@ajku.edu.pk

Kholoud Al-mugren − *Department of Physics, College of Sciences, Princess Nourah Bint Abdulrahman University, Riyadh 11144, Saudi Arabia*; Email: ksalmogren@pnu.edu.sa

Authors

Junaid Murtaza Awan − *Department of Chemistry, University of Azad Jammu and Kashmir, Muzaffarabad 13100 Azad Kashmir, Pakistan*

Muhammad Imran − *Department of Environmental Sciences, COMSATS University Islamabad, Vehari 61100, Pakistan*

Pervaiz Ahmad − *Department of Physics, University of Azad Jammu and Kashmir, 13100 Muzaffarabad, Pakistan*

Sirajul Haq − *Department of Chemistry, University of Azad Jammu and Kashmir, Muzaffarabad 13100 Azad Kashmir, Pakistan*

Sana Shakil − *Department of Chemistry, University of Azad Jammu and Kashmir, Muzaffarabad 13100 Azad Kashmir, Pakistan*

Satam Alotibi − *Department of Physics, College of Science and Humanities in Al-Kharj, Prince Sattam bin Abdulaziz University, Al-Kharj 11942, Saudi Arabia*

Abdulrahman I. Alharthi − *Department of Chemistry, College of Science and Humanities in Al-Kharj, Prince Sattam bin Abdulaziz University, Al-Kharj 11942, Saudi Arabia*

Muhammad Sarfraz Khan − *Department of Chemistry, University of Azad Jammu and Kashmir, Muzaffarabad 13100 Azad Kashmir, Pakistan*

Mayeen Uddin Khandaker − *Centre for Applied Physics and Radiation Technologies, School of Engineering and Technology, Sunway University, Bandar Sunway 47500 Selangor, Malaysia; Department of General Educational Development, Faculty of Science and Information Technology, Daffodil International University, Dhaka 1341, Bangladesh*; orcid.org/0000-0003-3772-294X

Complete contact information is available at: https://pubs.acs.org/10.1021/acsomega.3c04456

Author Contributions

Conceptualization, S.U.D. and S.H.; methodology, S.S., S.H., and P.A.; software, S.S., K.A., M.U.K., and M.I.; validation, K.A., M.S.K., and S.A.; formal analysis, J.M.A., S.A., and P.A.; investigation, M.I.; resources, S.U.D., P.A., and S.H.; data curation, M.I.; writing—original draft preparation, M.S.K., K.A., M.U.K., and S.U.D.; writing—review and editing, S.U.D., A.I.A., S.S., and K.A.; visualization, S.A. and M.U.K.; supervision, S.U.D.; project administration, S.H., S.U.D., and P.A. All authors have read and agreed to the published version of the manuscript.

Funding

Princess Nourah bint Abdulrahman University Researchers Supporting Project number (PNURSP2024 R10), Princess Nourah bint Abdulrahman University, Riyadh, Saudi Arabia

Notes

The authors declare no competing financial interest.

ACKNOWLEDGMENTS

Princess Nourah bint Abdulrahman University Researchers Supporting Project number (PNURSP2024 R10), Princess Nourah bint Abdulrahman University, Riyadh, Saudi Arabia

REFERENCES

(1) Drews, W.; Weber, G.; Tölg, G. Trace determination of nickel by microwave-induced plasma atomic emission spectrometry after preconcentration of nickel tetracarbonyl on Chromosorb. *Anal. Chim. Acta* **1990**, *231*, 265−271.

(2) Genchi, G.; Carocci, A.; Lauria, G.; Sinicropi, M. S.; Catalano, A. Nickel: Human health and environmental toxicology. *Int. J. Environ. Res. Public Health* **2020**, *17* (3), 679.

(3) Yang, S.; Li, J.; Shao, D.; Hu, J.; Wang, X. Adsorption of Ni (II) on oxidized multi-walled carbon nanotubes: effect of contact time, pH, foreign ions and PAA. *J. Hazard. Mater.* **2009**, *166* (1), 109−116.

(4) Organization, W. H. *Nickel in drinking water: background document for development of WHO Guidelines for drinking-water quality*; World Health Organization: 2021.

(5) Adhikari, S.; Yanuar, E.; Ng, D.-Q. Widespread nickel contamination in drinking water supplies of elementary schools in Taichung, Taiwan. *Environ. Sci. Pollut. Res.* **2022**, *29* (9), 12531−12539.

(6) Pereira, A. M.; Silva, L. J.; Simões, B. D.; Lino, C.; Pena, A. Exposure to nickel through commercial premade baby foods: Is there any risk? *J. Food Compos. Anal.* **2020**, *92*, No. 103541.

(7) Stevens, M.; Batlokwa, B. Removal of nickel (II) and cobalt (II) from wastewater using vinegar-treated eggshell waste biomass. *J. Water Resour. Protect.* **2017**, *9* (08), 931 DOI: 10.4236/jwarp.2017.98062.

(8) Zhang, X.; Liu, Y. Concurrent removal of Cu (II), Co (II) and Ni (II) from wastewater by nanostructured layered sodium vanadosilicate: Competitive adsorption kinetics and mechanisms. *J. Environ. Chem. Eng.* **2021**, *9* (5), No. 105945.

(9) Seet, R. C.; Johan, A.; Teo, C. E.; Gan, S. L.; Lee, K. H. Inhalational nickel carbonyl poisoning in waste processing workers. *Chest* **2005**, *128* (1), 424−429.

(10) Zhang, M.; Gao, B.; Yao, Y.; Inyang, M. Phosphate removal ability of biochar/MgAl-LDH ultra-fine composites prepared by liquid-phase deposition. *Chemosphere* **2013**, *92* (8), 1042−1047.

(11) Bardestani, R.; Roy, C.; Kaliaguine, S. The effect of biochar mild air oxidation on the optimization of lead (II) adsorption from wastewater. *J. Environ. Manage.* **2019**, *240*, 404−420.

(12) Din, S. U.; Khan, M. S.; Hussain, S.; Imran, M.; Haq, S.; Hafeez, M.; Rehman, F. U.; Chen, X. Adsorptive mechanism of chromium adsorption on siltstone−nanomagnetite−biochar composite. *J. Inorg. Organomet. Polym. Mater.* **2021**, *31*, 1608−1620.

(13) Igalavithana, A. D.; Mandal, S.; Niazi, N. K.; Vithanage, M.; Parikh, S. J.; Mukome, F. N.; Rizwan, M.; Oleszczuk, P.; Al-Wabel, M.; Bolan, N. Advances and future directions of biochar characterization methods and applications. *Crit. Rev. Environ. Sci. Technol.* **2017**, *47* (23), 2275−2330, DOI: 10.1080/10643389.2017.1421844.

(14) Alam, M. S.; Gorman-Lewis, D.; Chen, N.; Flynn, S. L.; Ok, Y. S.; Konhauser, K. O.; Alessi, D. S. Thermodynamic analysis of nickel (II) and zinc (II) adsorption to biochar. *Environ. Sci. Technol.* **2018**, *52* (11), 6246−6255.

(15) Iqbal, J.; Shah, N. S.; Sayed, M.; Niazi, N. K.; Imran, M.; Khan, J. A.; Khan, Z. U. H.; Hussien, A. G. S.; Polychronopoulou, K.; Howari, F. Nano-zerovalent manganese/biochar composite for the adsorptive and oxidative removal of Congo-red dye from aqueous solutions. *J. Hazard. Mater.* **2021**, *403*, No. 123854.

(16) Imran, M.; Iqbal, M. M.; Iqbal, J.; Shah, N. S.; Khan, Z. U. H.; Murtaza, B.; Amjad, M.; Ali, S.; Rizwan, M. Synthesis, characterization and application of novel MnO and CuO impregnated biochar composites to sequester arsenic (As) from water: modeling, thermodynamics and reusability. *J. Hazard. Mater.* **2021**, *401*, No. 123338.

(17) Chen, T.; Zhou, Z.; Xu, S.; Wang, H.; Lu, W. Adsorption behavior comparison of trivalent and hexavalent chromium on biochar derived from municipal sludge. *Bioresour. Technol.* **2015**, *190*, 388−394.
(18) Ye, L.; Peng, Z.; Wang, L.; Anzulevich, A.; Bychkov, I.; Tang, H.; Rao, M.; Zhang, Y.; Li, G.; Jiang, T. Preparation of core-shell iron ore-biochar composite pellets for microwave reduction. *Powder Technol.* **2018**, *338*, 365−375.
(19) Wu, S.-J.; Liou, T.-H.; Mi, F.-L. Synthesis of zero-valent copper-chitosan nanocomposites and their application for treatment of hexavalent chromium. *Bioresour. Technol.* **2009**, *100* (19), 4348−4353.
(20) Huang, X.; Li, M.; Friedli, H. R.; Song, Y.; Chang, D.; Zhu, L. Mercury emissions from biomass burning in China. *Environ. Sci. Technol.* **2011**, *45* (21), 9442−9448.
(21) Song, Z.; Lian, F.; Yu, Z.; Zhu, L.; Xing, B.; Qiu, W. Synthesis and characterization of a novel MnOx-loaded biochar and its adsorption properties for Cu2+ in aqueous solution. *Chem. Eng. J.* **2014**, *242*, 36−42.
(22) Fu, D.; Chen, Z.; Xia, D.; Shen, L.; Wang, Y.; Li, Q. A novel solid digestate-derived biochar-Cu NP composite activating H2O2 system for simultaneous adsorption and degradation of tetracycline. *Environ. Pollut.* **2017**, *221*, 301−310.
(23) Ghani, W. A. W. A. K.; Mohd, A.; da Silva, G.; Bachmann, R. T.; Taufiq-Yap, Y. H.; Rashid, U.; Ala', A. H. Biochar production from waste rubber-wood-sawdust and its potential use in C sequestration: chemical and physical characterization. *Ind. Crops Prod.* **2013**, *44*, 18−24.
(24) Jimenez, J.; Acda, M. N.; Razal, R. A.; Abasolo, W. P.; Hernandez, H. P.; Elepaño, A. R. Effect of tobacco stalk additive particle size on the bond strength and formaldehyde emission of urea formaldehyde bonded plywood. *Philipp. J. Sci.* **2020**, *149* (2), 333−342, DOI: 10.56899/149.02.11.
(25) Din, S. U.; Hussain, B.; Haq, S.; Imran, M.; Ahmad, P.; Khandaker, M. U.; Rehman, F. U.; Eldin, S. M.; Mousa, A. A. A.; Khan, I. Efficient arsenate decontamination from water using MgO-Itsit biochar composite: An equilibrium, kinetics and thermodynamic study. *Water* **2022**, *14* (21), 3559.
(26) Din, S. U.; Awan, J. M.; Imran, M.; Haq, S.; Hafeez, M.; Hussain, S.; Khan, M. S. Novel nanocomposite of biochar-zerovalent copper for lead adsorption. *Microsc. Res. Tech.* **2021**, *84* (11), 2598−2606.
(27) Erdoğan, S.; Önal, Y.; Akmil-Başar, C.; Bilmez-Erdemoğlu, S.; Sarıcı-Özdemir, Ç.; Köseoğlu, E.; Icduygu, G. Optimization of nickel adsorption from aqueous solution by using activated carbon prepared from waste apricot by chemical activation. *Appl. Surf. Sci.* **2005**, *252* (5), 1324−1331.
(28) Ghaee, A.; Shariaty-Niassar, M.; Barzin, J.; Zarghan, A. Adsorption of copper and nickel ions on macroporous chitosan membrane: Equilibrium study. *Appl. Surf. Sci.* **2012**, *258* (19), 7732−7743.
(29) Wang, J.; Liu, G.; Zhou, C.; Li, T.; Liu, J. Synthesis, characterization and aging study of kaolinite-supported zero-valent iron nanoparticles and its application for Ni (II) adsorption. *Mater. Res. Bull.* **2014**, *60*, 421−432.
(30) Montazer-Rahmati, M. M.; Rabbani, P.; Abdolali, A.; Keshtkar, A. R. Kinetics and equilibrium studies on biosorption of cadmium, lead, and nickel ions from aqueous solutions by intact and chemically modified brown algae. *J. Hazard. Mater.* **2011**, *185* (1), 401−407.
(31) Shakirullah, M.; Ahmad, I.; Shah, S.; Hameedullah. Sorption studies of nickel ions onto sawdust of *Dalbergia sissoo*. *J. Chin. Chem. Soc.* **2006**, *53* (5), 1045−1052, DOI: 10.1002/jccs.200600139.
(32) Yoon, K.; Cho, D.-W.; Bhatnagar, A.; Song, H. Adsorption of As (V) and Ni (II) by Fe-Biochar composite fabricated by co-pyrolysis of orange peel and red mud. *Environ. Res.* **2020**, *188*, No. 109809.
(33) Chaiyaraksa, C.; Boonyakiat, W.; Bukkontod, W.; Ngakom, W. Adsorption of Copper (II) and Nickel (II) by Chemical Modified Magnetic Biochar Derived from Eichhornia crassipes. *EnvironmentAsia* **2019**, *12* (2), 14 DOI: 10.14456/ea.2019.23.
(34) Richard, D.; Mucci, A.; Neculita, C. M.; Zagury, G. J. Comparison of organic materials for the passive treatment of synthetic neutral mine drainage contaminated by nickel: Adsorption and desorption kinetics and isotherms. *Water, Air, Soil Pollut.* **2020**, *231*, 556 DOI: 10.1007/s11270-020-04917-z.
(35) Vilvanathan, S.; Shanthakumar, S. Continuous biosorption of nickel from aqueous solution using Chrysanthemum indicum derived biochar in a fixed-bed column. *Water Sci. Technol.* **2017**, *76* (7), 1895−1906.
(36) Liu, L.; Guo, X.; Wang, S.; Li, L.; Zeng, Y.; Liu, G. Effects of wood vinegar on properties and mechanism of heavy metal competitive adsorption on secondary fermentation based composts. *Ecotoxicol. Environ. Saf.* **2018**, *150*, 270−279.
(37) Ali, U.; Shaaban, M.; Bashir, S.; Gao, R.; Fu, Q.; Zhu, J.; Hu, H. Rice straw, biochar and calcite incorporation enhance nickel (Ni) immobilization in contaminated soil and Ni removal capacity. *Chemosphere* **2020**, *244*, No. 125418.
(38) Fil, B. A.; Boncukcuoğlu, R.; Yilmaz, A. E.; Bayar, S. Adsorption of Ni (II) on ion exchange resin: Kinetics, equilibrium and thermodynamic studies. *Korean J. Chem. Eng.* **2012**, *29*, 1232−1238.
(39) Mahmoud, M. E.; Amira, M. F.; Seleim, S. M.; Mohamed, A. K. Adsorption isotherm models, kinetics study, and thermodynamic parameters of Ni (II) and Zn (II) removal from water using the LbL technique. *J. Chem. Eng. Data* **2017**, *62* (2), 839−850.
(40) Hu, X.; Xue, Y.; Liu, L.; Zeng, Y.; Long, L. Preparation and characterization of Na 2 S-modified biochar for nickel removal. *Environ. Sci. Pollut. Res.* **2018**, *25*, 9887−9895.
(41) Rajapaksha, A. U.; Vithanage, M.; Weerasooriya, R.; Dissanayake, C. Surface complexation of nickel on iron and aluminum oxides: A comparative study with single and dual site clays. *Colloids Surf., A* **2012**, *405*, 79−87.
(42) Green-Pedersen, H.; Jensen, B.; Pind, N. Nickel adsorption on MnO2, Fe (OH) 3, montmorillonite, humic acid and calcite: a comparative study. *Environ. Technol.* **1997**, *18* (8), 807−815.
(43) Ding, C.; Cheng, W.; Wang, X.; Wu, Z.-Y.; Sun, Y.; Chen, C.; Wang, X.; Yu, S.-H. Competitive sorption of Pb (II), Cu (II) and Ni (II) on carbonaceous nanofibers: a spectroscopic and modeling approach. *J. Hazard. Mater.* **2016**, *313*, 253−261.
(44) Gu, X.; Evans, L. J.; Barabash, S. J. Modeling the adsorption of Cd (II), Cu (II), Ni (II), Pb (II) and Zn (II) onto montmorillonite. *Geochim. Cosmochim. Acta* **2010**, *74* (20), 5718−5728.
(45) Marmier, N.; Delisée, A.; Fromage, F. Surface complexation modeling of Yb (III), Ni (II), and Cs (I) sorption on magnetite. *J. Colloid Interface Sci.* **1999**, *211* (1), 54−60.
(46) Gu, X.; Evans, L. J. Surface complexation modelling of Cd (II), Cu (II), Ni (II), Pb (II) and Zn (II) adsorption onto kaolinite. *Geochim. Cosmochim. Acta* **2008**, *72* (2), 267−276.
(47) Islam, M. A.; Awual, M. R.; Angove, M. J. A review on nickel (II) adsorption in single and binary component systems and future path. *J. Environ. Chem. Eng.* **2019**, *7* (5), No. 103305.
(48) Xu, Y.; Axe, L.; Boonfueng, T.; Tyson, T. A.; Trivedi, P.; Pandya, K. Ni (II) complexation to amorphous hydrous ferric oxide: an X-ray absorption spectroscopy study. *J. Colloid Interface Sci.* **2007**, *314* (1), 10−17.
(49) Zhao, X.; Qiang, S.; Wu, H.; Yang, Y.; Shao, D.; Fang, L.; Liang, J.; Li, P.; Fan, Q. Exploring the sorption mechanism of Ni (II) on Illite: batch sorption, modelling, EXAFS and extraction investigations. *Sci. Rep.* **2017**, *7* (1), 8495 DOI: 10.1038/s41598-017-09188-z.

https://doi.org/10.1021/acsomega.3c04456
ACS Omega 2023, 8, 39186−39193